Northumbria Research Link

Citation: Vo, Thuc and Lee, Jaehong (2011) Geometrical nonlinear analysis of thin-walled composite beams using finite element method based on first order shear deformation theory. Archive of Applied Mechanics, 81 (4). pp. 419-435. ISSN 0939-1533

Published by: Springer

URL: http://dx.doi.org/10.1007/s00419-010-0407-x <http://dx.doi.org/10.1007/s00419-010-0407-x>

This version was downloaded from Northumbria Research Link: http://nrl.northumbria.ac.uk/14092/

Northumbria University has developed Northumbria Research Link (NRL) to enable users to access the University's research output. Copyright © and moral rights for items on NRL are retained by the individual author(s) and/or other copyright owners. Single copies of full items can be reproduced, displayed or performed, and given to third parties in any format or medium for personal research or study, educational, or not-for-profit purposes without prior permission or charge, provided the authors, title and full bibliographic details are given, as well as a hyperlink and/or URL to the original metadata page. The content must not be changed in any way. Full items must not be sold commercially in any format or medium without formal permission of the copyright holder. The full policy is available online: http://nrl.northumbria.ac.uk/policies.html

This document may differ from the final, published version of the research and has been made available online in accordance with publisher policies. To read and/or cite from the published version of the research, please visit the publisher's website (a subscription may be required.)

www.northumbria.ac.uk/nrl

northumbria UNIVERSITY NEWCASTLE

Geometrical nonlinear analysis of thin-walled composite beams using finite element method based on first order shear deformation theory

Thuc Phuong Vo* and Jaehong Lee†

Department of Architectural Engineering, Sejong University
98 Kunja Dong, Kwangjin Ku, Seoul 143-747, Korea

(Dated: January 22, 2010)

Based on a seven-degree-of-freedom shear deformable beam model, a geometrical nonlinear analysis of thin-walled composite beams with arbitrary lay-ups under various types of loads is presented. This model accounts for all the structural coupling coming from both material anisotropy and geometric nonlinearity. The general nonlinear governing equations are derived and solved by means of an incremental Newton-Raphson method. A displacement-based one-dimensional finite element model that accounts for the geometric nonlinearity in the von Kármán sense is developed to solve the problem. Numerical results are obtained for thin-walled composite beam under vertical load to investigate the effects of fiber orientation, geometric nonlinearity and shear deformation on the axial-flexural-torsional response.

Keywords: Thin-walled composite beams; shear deformation; axial-flexural-torsional response; nonlinear theory.

I. INTRODUCTION

Fiber-reinforced composite materials have been used over the past few decades in various structures. Composites have many desirable characteristics, such as high ratio of stiffness and strength to weight, corrosion resistance and magnetic transparency. Thin-walled structural shapes made up of composite materials, which are usually produced by pultrusion, are being increasingly used in many engineering fields. A large number of practical problems of thin-walled composite structures require a geometrically nonlinear formulation, such as the post-buckling behavior, load carrying

*Postdoctoral research fellow

†Professor, corresponding author. Tel.:+82-2-3408-3287; fax:+82-2-3408-3331

; Electronic address: jhlee@sejong.ac.kr

capacity of structures used in aeronautical, aerospace as well as in mechanical and civil engineering. In such cases, linear finite element models are not able to predict the structural response accurately. Hence, the development of efficient and accurate nonlinear finite element models becomes crucial.

The geometrical nonlinear analysis of thin-walled composite beams has received considerable attention by researchers since the development of comprehensive theory of thin-walled bars by Vlasov [1] and Gjelsvik [2]. Bauld and Tzeng [3] presented nonlinear model for the balanced symmetric laminated composite materials by extending Gjelsvik's formulation. However, the formulation was somewhat not consistent in the sense that it used coordinate mapping when developing nonlinear stresses instead of variational formulation. Gupta and Rao [4,5] developed finite element analysis to study instability of thin-walled open-section composite beams. The nonlinear expressions for the strains occurring in these members under axial, flexural and torsional loads, were incorporated in a general instability analysis. A finite element formulation was developed by Stemple and Lee [6,7] to take into account the warping effect of composite beams undergoing large deflection or finite rotation. By extending model of Bauld and Tzeng [3], Omidvar and Ghorbanpoor [8] derived a nonlinear finite element analysis of thin-walled open-section composite beams with symmetric lay-up based on the updated Lagrangian formulation. Fraternali and Feo [9] formulated a small strain and moderate rotation theory of thin-walled composite beams by generalizing the classical Vlasov theory. This beam model accounted for axial, bending, torsion and warping deformations and allowed one to predict critical loads and initial post-buckling behavior. Rajasekaran and Nalinaa [10] presented the formulation for static, bucking and vibration analysis of non-prismatic thin-walled composite spatial members of generic section. The theory was limited to small strains, moderate deflections and small rotations. Bhaskar, Librescu and Song [11,12] developed non-linear theory of thin-walled composite beams, which was employed in a broad field of engineering problems. In this model, the transverse shear deformation was taken into account but the warping torsion component was neglected. Special attention deserved the works of Machado, Cortinez and Piovan [13,14] who introduced a geometrically non-linear theory for analyzing the stability of thin-walled composite beams. This model applied for both open and closed cross-sections and took into account shear flexibility (bending and warping shear). However, it was strictly valid for symmetric balanced laminates and especially orthotropic laminates. Sapountzakis and Panagos [15] introduced the non-linear analysis of a composite Timoshenko beam with arbitrary variable cross section undergoing moderate large deflections by employing the analog equation method, a boundary element method (BEM)-based method. Cardoso et al. [16] developed two-node Hermitean finite beam elements, with seven-degree-of-freedom per node for structural analysis of thin-walled composite beams with geometrically nonlinear behavior, including post-critical behavior and

warping deformation.

In this paper, which is an extension of the authors' previous works [17,18], a geometrically nonlinear model for thin-walled composite beams with arbitrary lay-ups under various types of loads is presented. This model is based on the first-order shear deformable beam theory, and accounts for all the structural coupling coming from both material anisotropy and geometric nonlinearity. The general nonlinear governing equations are derived and solved by means of an incremental Newton-Raphson method. A displacement-based one-dimensional finite element model with seven-degree-of-freedom per node that accounts for the geometric nonlinearity in the von Kármán sense is developed to solve the problem. Numerical results are obtained for thin-walled composite beam under vertical load to investigate the effects of fiber orientation, geometric nonlinearity and shear deformation on the axial-flexural-torsional response.

II. KINEMATICS

The theoretical developments presented in this paper require two sets of coordinate systems which are mutually interrelated. The first coordinate system is the orthogonal Cartesian coordinate system (x, y, z), for which the x and y axes lie in the plane of the cross section and the z axis parallel to the longitudinal axis of the beam. The second coordinate system is the local plate coordinate system (n, s, z) as shown in Fig.1, wherein the n axis is normal to the middle surface of a plate element, the s axis is tangent to the middle surface and is directed along the contour line of the cross section. The (n, s, z) and (x, y, z) coordinate systems are related through an angle of orientation ψ. As defined in Fig.1, a point P, called the pole, is placed at an arbitrary point x_p, y_p. A line through P parallel to the z axis is called the pole axis.

To derive the analytical model for thin-walled composite beams, the following assumptions are made:

1. The contour of the thin wall does not deform in its own plane.

2. Transverse shear strains $\gamma_{xz}^{\circ}, \gamma_{yz}^{\circ}$ and warping shear strain γ_{ω}° are incorporated. It is assumed that they are uniform over the cross-sections.

According to assumption 1, the midsurface displacement components $\bar{u}, \bar{v}$ at a point A in the contour coordinate system can be expressed in terms of a displacements U, V of the pole P in the x, y directions, respectively, and the rotation angle Φ about the pole axis,

$$\bar{u}(s,z) = U(z)\sin\psi(s) - V(z)\cos\psi(s) - \Phi(z)q(s) \tag{1a}$$

$$\bar{v}(s,z) = U(z)\cos\psi(s) + V(z)\sin\psi(s) + \Phi(z)r(s) \tag{1b}$$

These equations apply to the whole contour. The out-of-plane shell displacement $\bar{w}$ can now be found from the assumption 2. For each element of middle surface, the midsurface shear strains in the contour can be expressed with respect to the transverse shear and warping shear strains.

$$\bar{\gamma}_{nz}(s,z) = \gamma^{\circ}_{xz}(z)\sin\psi(s) - \gamma^{\circ}_{yz}(z)\cos\psi(s) - \gamma^{\circ}_{\omega}(z)q(s) \tag{2a}$$

$$\bar{\gamma}_{sz}(s,z) = \gamma^{\circ}_{xz}(z)\cos\psi(s) + \gamma^{\circ}_{yz}(z)\sin\psi(s) + \gamma^{\circ}_{\omega}(z)r(s) \tag{2b}$$

Further, it is assumed that midsurface shear strain in $s-n$ direction is zero ($\bar{\gamma}_{sn}=0$). From the definition of the shear strain, $\bar{\gamma}_{sz}=0$ can also be given for each element of middle surface as:

$$\bar{\gamma}_{sz}(s,z) = \frac{\partial\bar{v}}{\partial z} + \frac{\partial\bar{w}}{\partial s} \tag{3}$$

Displacement $\bar{w}$ can be integrated with respect to s from the origin to an arbitrary point on the contour,

$$\bar{w}(s,z) \;=\; W(z) + \Psi_y(z)x(s) + \Psi_x(z)y(s) + \Psi_\omega(z)\omega(s) \tag{4}$$

where Ψ_x, Ψ_y and Ψ_ω represent rotations of the cross section with respect to x, y and ω, respectively, given by:

$$\Psi_y \;=\; \gamma^{\circ}_{xz}(z) - U' \tag{5a}$$

$$\Psi_x \;=\; \gamma^{\circ}_{yz}(z) - V' \tag{5b}$$

$$\Psi_\omega \;=\; \gamma^{\circ}_{\omega}(z) - \Phi' \tag{5c}$$

When the shear deformation effect is ignored, Eq.(5) degenerates to $\Psi_y = -U'$, $\Psi_x = -V'$ and $\Psi_\omega = -\Phi'$. As a result, the number of unknown variables reduces to four leading to the Euler-Bernoulli beam model. The prime ($'$) is used to indicate differentiation with respect to z and ω is the so-called sectorial coordinate or warping function given by

$$\omega(s) \;=\; \int_{s_\circ}^{s} r(s)ds \tag{6}$$

The displacement components u, v, w representing the deformation of any generic point on the profile section are given with respect to the midsurface displacements $\bar{u}, \bar{v}, \bar{w}$ by assuming the first order variation of inplane displacements v, w through the thickness of the contour as:

$$u(s,z,n) \;=\; \bar{u}(s,z) \tag{7a}$$

$$v(s,z,n) \;=\; \bar{v}(s,z) + n\bar{\psi}_s(s,z) \tag{7b}$$

$$w(s,z,n) \;=\; \bar{w}(s,z) + n\bar{\psi}_z(s,z) \tag{7c}$$

where, $\bar{\psi}_s$ and $\bar{\psi}_z$ denote the rotations of a transverse normal about the z and s axis, respectively. These functions can be determined by considering that the midsurface shear strains $\bar{\gamma}_{nz}$ is given by definition:

$$\bar{\gamma}_{nz}(s,z) = \frac{\partial \bar{w}}{\partial n} + \frac{\partial \bar{u}}{\partial z} \tag{8}$$

By comparing Eq.(2) and (8), the function $\bar{\psi}_z$ can be written as

$$\bar{\psi}_z = \Psi_y \sin\psi - \Psi_x \cos\psi - \Psi_\omega q \tag{9}$$

Similarly, using the assumption that the shear strain γ_{sn} should vanish at midsurface, the function $\bar{\psi}_s$ can be obtained

$$\bar{\psi}_s = -\frac{\partial \bar{u}}{\partial s} \tag{10}$$

The von Kármán type strains, in which only the products of u, v, and their derivatives are retained and all other nonlinear terms are neglected are given by

$$\epsilon_z(s,z,n) = \frac{\partial w}{\partial z} + \frac{1}{2}\Big[\big(\frac{\partial u}{\partial z}\big)^2 + \big(\frac{\partial v}{\partial z}\big)^2\Big] \tag{11a}$$

$$\gamma_{sz}(s,z,n) = \frac{\partial v}{\partial z} + \frac{\partial w}{\partial s} \tag{11b}$$

$$\gamma_{nz}(s,z,n) = \frac{\partial w}{\partial n} + \frac{\partial u}{\partial z} \tag{11c}$$

By substituting Eqs.(1), (4) and (7) into Eq.(11), and using the following relations

$$x - x_p = q\cos\psi + r\sin\psi \tag{12a}$$

$$y - y_p = q\sin\psi - r\cos\psi \tag{12b}$$

Eq.(11) can be rewritten as

$$\epsilon_z = \bar{\epsilon}_z + n\bar{\kappa}_z + n^2\bar{\chi}_z \tag{13a}$$

$$\gamma_{sz} = \bar{\gamma}_{sz} + n\bar{\kappa}_{sz} \tag{13b}$$

$$\gamma_{nz} = \bar{\gamma}_{nz} + n\bar{\kappa}_{nz} \tag{13c}$$

where

$$\bar{\epsilon}_z = \frac{\partial \bar{w}}{\partial z} + \frac{1}{2}\Big[\big(\frac{\partial \bar{u}}{\partial z}\big)^2 + \big(\frac{\partial \bar{v}}{\partial z}\big)^2\Big] \tag{14a}$$

$$\bar{\kappa}_z = -\frac{\partial^2 \bar{u}}{\partial z^2} - 2\frac{\partial^2 \bar{u}}{\partial s \partial z}\frac{\partial \bar{v}}{\partial z} \tag{14b}$$

$$\bar{\kappa}_{sz} = -2\frac{\partial^2 \bar{u}}{\partial s \partial z} \tag{14c}$$

$$\bar{\chi}_z = \Big(\frac{\partial^2 \bar{u}}{\partial s \partial z}\Big)^2 \tag{14d}$$

In Eq.(14), $\bar{\epsilon}_z$, $\bar{\kappa}_z, \bar{\kappa}_{sz}$ and $\bar{\chi}_z$ are midsurface axial strain and biaxial curvature of the shell, respectively. The above shell strains can be converted to beam strain components by substituting Eqs.(1), (4) and (7) into Eq.(14) as

$$\bar{\epsilon}_z = \epsilon_z^\circ + x\kappa_y + y\kappa_x + \omega\kappa_\omega \tag{15a}$$

$$\bar{\kappa}_z = \kappa_y \sin\psi - \kappa_x \cos\psi - \kappa_\omega q + 2\chi_z r \tag{15b}$$

$$\bar{\kappa}_{sz} = \kappa_{sz} \tag{15c}$$

$$\bar{\chi}_z = \chi_z \tag{15d}$$

where $\epsilon_z^\circ, \kappa_x, \kappa_y, \kappa_\omega, \kappa_{sz}$ and χ_z are axial strain, biaxial curvatures in the x and y direction, warping curvature with respect to the shear center, twisting and high order curvature in the beam, respectively defined as

$$\epsilon_z^\circ = W' + \frac{1}{2}\left[U'^2 + V'^2 + (r^2+q^2)\Phi'^2\right] - x_p V'\Phi' + y_p U'\Phi' \tag{16a}$$

$$\kappa_x = \Psi_x' - U'\Phi' \tag{16b}$$

$$\kappa_y = \Psi_y' + V'\Phi' \tag{16c}$$

$$\kappa_\omega = \Psi_\omega' \tag{16d}$$

$$\kappa_{sz} = \Phi' - \Psi_\omega \tag{16e}$$

$$\chi_z = \frac{1}{2}\Phi'^2 \tag{16f}$$

The resulting strains can be obtained from Eqs.(13) and (15) as

$$\epsilon_z = \epsilon_z^\circ + (x + n\sin\psi)\kappa_y + (y - n\cos\psi)\kappa_x + (\omega - nq)\kappa_\omega + (2rn + n^2)\chi_z \tag{17a}$$

$$\gamma_{sz} = \gamma_{xz}^\circ \cos\psi + \gamma_{yz}^\circ \sin\psi + \gamma_\omega^\circ r + n\kappa_{sz} \tag{17b}$$

$$\gamma_{nz} = \gamma_{xz}^\circ \sin\psi - \gamma_{yz}^\circ \cos\psi - \gamma_\omega^\circ q \tag{17c}$$

III. VARIATIONAL FORMULATION

Total potential energy of the system is calculated by sum of strain energy and potential energy

$$\Pi = \mathcal{U} + \mathcal{V} \tag{18}$$

where $\mathcal{U}$ is the strain energy

$$\mathcal{U} = \frac{1}{2}\int_v (\sigma_z\epsilon_z + \sigma_{sz}\gamma_{sz} + \sigma_{nz}\gamma_{nz})dv \tag{19}$$

The strain energy is calculated by substituting Eq.(17) into Eq.(19)

$$\begin{aligned}\mathcal{U} &= \frac{1}{2}\int_v \Big\{\sigma_z\Big[\epsilon_z^\circ + (x+n\sin\psi)\kappa_y + (y-n\cos\psi)\kappa_x + (\omega-nq)\kappa_\omega + (2rn+n^2)\chi_z\Big] \\ &+ \sigma_{sz}\Big[\gamma_{xz}^\circ\cos\psi + \gamma_{yz}^\circ\sin\psi + \gamma_\omega^\circ r + n\kappa_{sz}\Big] + \sigma_{nz}\Big[\gamma_{xz}^\circ\sin\psi - \gamma_{yz}^\circ\cos\psi - \gamma_\omega^\circ q\Big]\Big\}dv \end{aligned} \tag{20}$$

The variation of the strain energy, Eq.(20), can be stated as

$$\delta\mathcal{U} = \int_0^l (N_z\delta\epsilon_z + M_y\delta\kappa_y + M_x\delta\kappa_x + M_\omega\delta\kappa_\omega + V_x\delta\gamma_{xz}^\circ + V_y\delta\gamma_{yz}^\circ + T\delta\gamma_\omega^\circ + M_t\delta\kappa_{sz} + R_z\delta\chi_z)dz \tag{21}$$

where $N_z, M_x, M_y, M_\omega, V_x, V_y, T, M_t$ and R_z are axial force, bending moments in the x and y directions, warping moment (bimoment), shear force in the x and y directions, warping torque, torsional moment and the high order stress resultant with respect to the centroid respectively, defined by integrating over the cross-sectional area A as

$$N_z = \int_A \sigma_z dsdn \tag{22a}$$
$$M_y = \int_A \sigma_z(x+n\sin\psi)dsdn \tag{22b}$$
$$M_x = \int_A \sigma_z(y-n\cos\psi)dsdn \tag{22c}$$
$$M_\omega = \int_A \sigma_z(\omega-nq)dsdn \tag{22d}$$
$$V_x = \int_A (\sigma_{sz}\cos\psi + \sigma_{nz}\sin\psi)dsdn \tag{22e}$$
$$V_y = \int_A (\sigma_{sz}\sin\psi - \sigma_{nz}\cos\psi)dsdn \tag{22f}$$
$$T = \int_A (\sigma_{sz}r - \sigma_{nz}q)dsdn \tag{22g}$$
$$M_t = \int_A \sigma_{sz}ndsdn \tag{22h}$$
$$R_z = \int_A \sigma_z(2rn+n^2)dsdn \tag{22i}$$

The variation of the strain energy can be obtained by substituting Eqs.(16) and (17) into Eq.(21)

$$\begin{aligned}\delta\mathcal{U} &= \int_0^l \Big[N_z\delta W' + M_y\delta\Psi_y' + M_x\delta\Psi_x' + M_\omega\delta\Psi_\omega' + V_x\delta(U'+\Psi_y) + V_y\delta(V'+\Psi_x) \\ &+ T\delta(\Phi'+\Psi_\omega) + M_t\delta(\Phi'-\Psi_\omega) + N_z(U'\delta U' + V'\delta V') \\ &+ (M_y - x_pN_z)(V'\delta\Phi' + \Phi'\delta V') - (M_x - y_pN_z)(U'\delta\Phi' + \Phi'\delta U') + (r_p^2N_z + R_z)\Phi'\delta\Phi'\Big]dz \end{aligned} \tag{23}$$

On the other hand, the variation of work done by external forces can be written as

$$\delta\mathcal{V} = -\int_v (p_z\delta w + p_n\delta u + p_s\delta v)dv \tag{24}$$

where p_z, p_n, p_s are forces acting in z, n and s direction.

The above expression can be written with respect to the shell forces and displacements by using Eq.(7)

$$\delta\mathcal{V} = -\int_0^l \int_s (\bar{p}_z\delta\bar{w} + \bar{p}_n\delta\bar{u} + \bar{p}_s\delta\bar{v} + \bar{m}_z\bar{\psi}_z + \bar{m}_s\bar{\psi}_s)dsdz \tag{25}$$

where $\bar{p}_z, \bar{p}_s, \bar{m}_z, \bar{m}_s, \bar{p}_n$ are shell forces defined by

$$(\bar{p}_z, \bar{m}_z) = \int_n p_z(1,n)dn \tag{26a}$$

$$(\bar{p}_s, \bar{m}_s) = \int_n p_s(1,n)dn \tag{26b}$$

$$\bar{p}_n = \int_n p_n dn \tag{26c}$$

After substituting Eqs.(1) and (4) into Eq.(25), the variation of the work done by the external forces can be written with respect to the bar forces

$$\delta\mathcal{V} = -\int_0^l (\mathcal{P}_z\delta W + \mathcal{V}_x\delta U + \mathcal{M}_y\delta\Psi_y + \mathcal{V}_y\delta V + \mathcal{M}_x\delta\Psi_x + \mathcal{T}\delta\Phi + \mathcal{M}_\omega\delta\Psi_\omega)dz \tag{27}$$

where the bar forces are related to the shell forces as

$$\mathcal{P}_z = \int_s \bar{p}_z ds \tag{28a}$$

$$\mathcal{V}_y = \int_s (\bar{p}_s\sin\psi - \bar{p}_n\cos\psi)ds \tag{28b}$$

$$\mathcal{V}_x = \int_s (\bar{p}_s\cos\psi + \bar{p}_n\sin\psi)ds \tag{28c}$$

$$\mathcal{T} = \int_s (\bar{p}_s r - \bar{p}_n q + \bar{m}_s)ds \tag{28d}$$

$$\mathcal{M}_y = \int_s (\bar{m}_z\sin\psi + \bar{p}_z x)ds \tag{28e}$$

$$\mathcal{M}_x = \int_s (-\bar{m}_z\cos\psi + \bar{p}_z y)ds \tag{28f}$$

$$\mathcal{M}_\omega = \int_s (-\bar{m}_z q + \bar{p}_z\omega)ds \tag{28g}$$

Using the principle that the variation of the total potential energy is zero, the weak form of the present theory for thin-walled composite beams is given by

$$\begin{aligned} 0 = & \int_0^l \Big[N_z\delta W' + M_y\delta\Psi_y' + M_x\delta\Psi_x' + M_\omega\delta\Psi_\omega' + V_x\delta(U'+\Psi_y) + V_y\delta(V'+\Psi_x) \\ & + T\delta(\Phi'+\Psi_\omega) + M_t\delta(\Phi'-\Psi_\omega) + N_z(U'\delta U' + V'\delta V') \\ & + (M_y - x_pN_z)(V'\delta\Phi' + \Phi'\delta V') - (M_x - y_pN_z)(U'\delta\Phi' + \Phi'\delta U') + (r_p^2N_z + R_z)\Phi'\delta\Phi' \\ & - \mathcal{P}_z\delta W - \mathcal{V}_x\delta U - \mathcal{M}_y\delta\Psi_y - \mathcal{V}_y\delta V - \mathcal{M}_x\delta\Psi_x - \mathcal{T}\delta\Phi - \mathcal{M}_\omega\delta\Psi_\omega\Big]dz \end{aligned} \tag{29}$$

IV. CONSTITUTIVE EQUATIONS

The constitutive equations of a k^{th} orthotropic lamina in the laminate co-ordinate system of section are given by

$$\left\{ \begin{array}{c} \sigma_z \\ \sigma_{sz} \end{array} \right\}^k = \left[\begin{array}{cc} \bar{Q}^*_{11} & \bar{Q}^*_{16} \\ \bar{Q}^*_{16} & \bar{Q}^*_{66} \end{array} \right]^k \left\{ \begin{array}{c} \epsilon_z \\ \gamma_{sz} \end{array} \right\} \tag{30}$$

where $\bar{Q}^*_{ij}$ are transformed reduced stiffnesses. The transformed reduced stiffnesses can be calculated from the transformed stiffnesses based on the plane stress ($\sigma_s = 0$) and plane strain ($\epsilon_s = 0$) assumption. More detailed explanation can be found in Ref.[19].

The constitutive relation for out-of-plane stress and strain is given by

$$\sigma_{nz} = \bar{Q}_{55}\gamma_{nz} \tag{31}$$

The constitutive equations for bar forces and bar strains are obtained by using Eqs.(17), (22) and (30)

$$\left\{ \begin{array}{c} N_z \\ M_y \\ M_x \\ M_\omega \\ M_t \\ V_x \\ V_y \\ T \\ R_z \end{array} \right\} = \left[\begin{array}{ccccccccc} E_{11} & E_{12} & E_{13} & E_{14} & E_{15} & E_{16} & E_{17} & E_{18} & E_{19} \\ & E_{22} & E_{23} & E_{24} & E_{25} & E_{26} & E_{27} & E_{28} & E_{29} \\ & & E_{33} & E_{34} & E_{35} & E_{36} & E_{37} & E_{38} & E_{39} \\ & & & E_{44} & E_{45} & E_{46} & E_{47} & E_{48} & E_{49} \\ & & & & E_{55} & E_{56} & E_{57} & E_{58} & E_{59} \\ & & & & & E_{66} & E_{67} & E_{68} & E_{69} \\ & & & & & & E_{77} & E_{78} & E_{79} \\ & & & & & & & E_{88} & E_{89} \\ \text{sym.} & & & & & & & & E_{99} \end{array} \right] \left\{ \begin{array}{c} \epsilon^\circ_z \\ \kappa_y \\ \kappa_x \\ \kappa_\omega \\ \kappa_{sz} \\ \gamma^\circ_{xz} \\ \gamma^\circ_{yz} \\ \gamma^\circ_\omega \\ \chi_z \end{array} \right\} \tag{32}$$

where E_{ij} are the laminate stiffnesses of thin-walled composite beams. ($E_{i,9} \quad i = 1..9$) can be defined by

$$E_{19} = \int_s (2rB_{11} + D_{11})ds \tag{33a}$$

$$E_{29} = \int_s \Big[2rxB_{11} + D_{11}(x + 2r\sin\psi) + F_{11}\sin\psi\Big]ds \tag{33b}$$

$$E_{39} = \int_s \Big[2ryB_{11} + D_{11}(y - 2r\cos\psi) - F_{11}\cos\psi\Big]ds \tag{33c}$$

$$E_{49} = \int_s \Big[2r\omega B_{11} + D_{11}(\omega - 2rq) - F_{11}q\Big]ds \tag{33d}$$

$$E_{59} = \int_s (2rD_{16} + F_{16})ds \tag{33e}$$

$$E_{69} = \int_s (2rB_{16} + D_{16})\cos\psi ds \tag{33f}$$

$$E_{79} = \int_s (2rB_{16} + D_{16}) \sin\psi ds \tag{33g}$$

$$E_{89} = \int_s (2rB_{16} + D_{16}) r ds \tag{33h}$$

$$E_{99} = \int_s (4r^2 D_{11} + 4rF_{11} + H_{11}) ds \tag{33i}$$

where A_{ij}, B_{ij}, D_{ij} are the extensional, coupling, bending stiffness matrices and F_{ij}, H_{ij} are the higher order stiffness matrices, respectively, defined by

$$(A_{ij}, B_{ij}, D_{ij}, F_{ij}, H_{ij}) = \int \bar{Q}_{ij}(1, n, n^2, n^3, n^4) dn \tag{34}$$

Other values of the laminate stiffnesses E_{ij} can be found in Ref.[17].

V. GOVERNING EQUATIONS

The nonlinear equilibrium equations of the present study can be obtained by integrating the derivatives of the varied quantities by parts and collecting the coefficients of $\delta W, \delta U, \delta V, \delta\Phi, \delta\Psi_y, \delta\Psi_x$ and $\delta\Psi_\omega$

$$N_z' + \mathcal{P}_z = 0 \tag{35a}$$

$$V_x' + [N_z(U' + y_p\Phi')]' - [M_x\Phi']' + \mathcal{V}_x = 0 \tag{35b}$$

$$V_y' + [N_z(V' - x_p\Phi')]' + [M_y\Phi']' + \mathcal{V}_y = 0 \tag{35c}$$

$$M_t' + T' + [N_z(r_p^2\Phi' + y_pU' - x_pV')]' + [M_yV']' - [M_xU']' + [R_z\Phi']' + \mathcal{T} = 0 \tag{35d}$$

$$M_y' - V_x + \mathcal{M}_y = 0 \tag{35e}$$

$$M_x' - V_y + \mathcal{M}_x = 0 \tag{35f}$$

$$M_\omega' + M_t - T + \mathcal{M}_\omega = 0 \tag{35g}$$

The natural boundary conditions are of the form

$$\delta W : N_z \tag{36a}$$

$$\delta U : V_x + N_z(U' + y_p\Phi') - M_x\Phi' \tag{36b}$$

$$\delta V : V_y + N_z(V' - x_p\Phi') + M_y\Phi' \tag{36c}$$

$$\delta\Phi : T + M_t + N_z(r_p^2\Phi' + y_pU' - x_pV') + M_yV' - M_xU' + R_z\Phi' \tag{36d}$$

$$\delta\Psi_y : M_y \tag{36e}$$

$$\delta\Psi_x : M_x \tag{36f}$$

$$\delta\Psi_\omega : M_\omega \tag{36g}$$

Eq.(36g) denotes the warping restraint boundary condition. When the warping of the cross section is restrained, $\Psi_\omega = 0$ and when the warping is not restrained, $M_\omega = 0$.

By substituting Eqs.(16) and (32) into Eq.(35), the explicit form of the governing equations can be expressed with respect to the laminate stiffnesses E_{ij}. Eq.(35) is the most general nonlinear equations for axial, flexural, torsional and shearing behavior of thin-walled composite beams under various types of loads, and the dependent variables, W, U, V, Φ, Ψ_x, Ψ_y and Ψ_ω are fully coupled.

VI. FINITE ELEMENT FORMULATION

The present theory for thin-walled composite beams described in the previous section was implemented via a one-dimensional displacement-based finite element method. The linear, quadratic and cubic elements with seven degrees of freedom at each node are derived. The same interpolation function is used for all the translational and rotational displacements. The generalized displacements are expressed over each element as a combination of the one-dimensional Lagrange interpolation function $\widehat{\phi_j}$ associated with node j and the nodal values

$$W = \sum_{j=1}^{n} w_j \widehat{\phi_j} \tag{37a}$$

$$U = \sum_{j=1}^{n} u_j \widehat{\phi_j} \tag{37b}$$

$$V = \sum_{j=1}^{n} v_j \widehat{\phi_j} \tag{37c}$$

$$\Phi = \sum_{j=1}^{n} \phi_j \widehat{\phi_j} \tag{37d}$$

$$\Psi_y = \sum_{j=1}^{n} \psi_{yj} \widehat{\phi_j} \tag{37e}$$

$$\Psi_x = \sum_{j=1}^{n} \psi_{xj} \widehat{\phi_j} \tag{37f}$$

$$\Psi_\omega = \sum_{j=1}^{n} \psi_{\omega j} \widehat{\phi_j} \tag{37g}$$

where n is the number of nodes in an element and Lagrange interpolation function $\widehat{\phi_j}$ for linear, quadratic and cubic elements are available in the literature.

Substituting these expressions into the weak statement in Eq.(29), the finite element model of a typical element can be expressed as

$$\big[K(\{\Delta\})\big]\{\Delta\} = \{f\} \tag{38}$$

The nonlinear algebraic equations of present theory are solved by an iterative method. Thus, the nonlinear equations are linearized by evaluating the nonlinear terms with the known solution from preceding iterations. The Newton−Raphson method that uses the tangent stiffness matrix, which is symmetric for all structural problems, is used in this study. By using this method, solution of Eq.(38) results in the following linearized equations for the incremental solution at the r^{th} iteration (Reddy [20])

$$\left[T\{\Delta\}^{r-1}\right]\{\Delta\} = \{f\} - ([K]\{\Delta\}^{r-1} \tag{39}$$

where the tangent stiffness matrix is defined by

$$T_{ij}^{\alpha\beta} = \frac{\partial K_{ik}^{\alpha\gamma}}{\partial u_j^{\beta}} u_k^{\gamma} + K_{ij}^{\alpha\beta} \tag{40}$$

In Eq.(38), $\{\Delta\}$ is the unknown nodal displacements

$$\{\Delta\} = \{W\ U\ V\ \Phi\ \Psi_y\ \Psi_x\ \Psi_\omega\}^{\mathrm{T}} \tag{41}$$

VII. NUMERICAL EXAMPLES

Throughout the numerical examples, a tolerance of $\epsilon = 10^{-3}$ and maximum allowable iterations of 20 (per load step) are used to check for the convergence of nodal displacements in the Newton−Raphson iteration scheme. The initial solution vector is chosen to be the zero vector, so that the first iteration solution corresponds to the linear solution. Plane stress assumption ($\sigma_s = 0$) is used in the numerical computation.

For verification purpose, the buckling behavior of a cantilever and simply supported symmetrically laminated mono-symmetric I-beam with length $L = 1.0$m under axial force at the centroid is performed. The top and bottom flange widths are 30mm and 50mm and web height are 50mm, respectively. The flanges and web are made of sixteen layers with each layer 0.13mm in thickness. All computations are carried out for the glass-epoxy materials with the following material properties: $E_1 = 53.78$GPa , $E_2 = E_3 = 17.93$GPa , $G_{12} = G_{13} = 8.96$GPa , $G_{23} = 3.45$GPa , $\nu_{12} = 0.25$. The critical buckling loads obtained from present model are compared with those of Kim et al. [21] and Vo and Lee [22], which are based on the linear bifurcation buckling analysis and ABAQUS solution [23]. The results of the different methods are found to be in a good agreement in Table I. Load versus the lateral displacement of two fiber angles $\theta = 30^\circ$ and 60° in the flanges and web with different values of initial loading imperfections in x-direction ($V_x = 0.5 \times 10^{-3} V_z$, $1.0 \times 10^{-3} V_z$ and $2.5 \times 10^{-3} V_z$) are plotted in Figs. 2 and 3. These load-displacement curves monotonically increase and approach a linear bifurcation buckling load, which is characteristic of an incipient limit-

point response of the beam. This response is also justified by the fact that the value of the limit-point load decreases with increasing imperfection amplitude.

In order to demonstrate the accuracy of this study further, a cantilever doubly symmetric composite I-beam with length $L = 0.5$m under a tip vertical load P=2000N at the free end is investigated. Lay-ups and material properties are the same with previous example except the geometry of I-section. Both of flanges width and web height are 50mm. For comparison, the axial and vertical displacements at the free end by this study and the results by 600 nine-noded ABAQUS's shell elements (S9R5) are presented. The accuracy of the prediction from present model with the ABAQUS solution can be seen again in Table II for all lamination schemes considered.

A pinned-hinged composite I-beam of length $L = 2$m under an eccentric uniform load q acting at the left of the top flange is considered in order to investigate the effects of fiber orientation, geometric nonlinearity and shear deformation on the axial-flexural-torsional response. The geometry and stacking sequence of composite I-beam is shown in Fig.4 and the following engineering constants are used

$$E_1/E_2 = 25, G_{12}/E_2 = 0.6, G_{12} = G_{13} = G_{23}, \nu_{12} = 0.25 \tag{42}$$

For convenience, the following nondimensional values of the axial, lateral, vertical displacement and load parameter are used

$$\overline{w} = \frac{w}{b_2} \tag{43a}$$

$$\overline{u} = \frac{w}{b_2} \tag{43b}$$

$$\overline{v} = \frac{v}{b_2} \tag{43c}$$

$$\overline{q} = \frac{qL^4}{E_2 b_2^3 t} \tag{43d}$$

Stacking sequence of this beam consists of four layers with equal thickness as follows: $[\theta/-\theta]_s$ at the bottom flange and unidirectional at the web and top flange, respectively. Although the lay-up of each flange and web is locally symmetric, the behavior of global section is unsymmetrical and thus, the coupling stiffnesses E_{19} and E_{68} do not vanish. Accordingly, this beam sustains two kinds of couplings from material anisotropy and geometric nonlinearity simultaneously. The load with increment of $\Delta\overline{q} = 0.015$ is increased until the first critical point is reached. It can be observed in Fig.5 that the highest load decreases monotonically with the increasing of fiber angle and is about eight times when fiber angle is varied from $\theta = 0^\circ$ to $\theta = 90^\circ$. Based on the result of this figure, an applied load $\overline{q} = 1.75$ is chosen to show effect of fiber orientation on the axial-flexural-torsional response. The solution of the linear analysis is also presented to highlight the difference between linear and nonlinear response.

Axial and horizontal displacements with respect to fiber angle variation are plotted in Fig.6. It should be noted that no linear axial and lateral displacements $\overline{w}, \overline{u}$ are seen for all fiber angles because they are decoupled with vertical and torsional load. The vertical displacement with respect to fiber angle variation is demonstrated in Fig.7. By using a combination of one-dimensional linear Lagrange and Hermite-cubic interpolation function in finite element formulation, the results obtained from previous research [24] based on the classical beam theory are also displayed. The discrepancy of vertical displacement due to the shear deformation effect is remarkable and should not be ignored in nonlinear analysis especially for the higher fiber angles. As fiber angle is less than $\theta = 30^\circ$, the vertical displacement of linear and nonlinear analysis coincides. However, as the fiber angle increases, since the geometrical nonlinear effect is prominent, the discrepancy between the linear and nonlinear analysis becomes significant. From the aforementioned figures, it can be observed that the difference between displacements of two analyzes is minimum at fiber angle $\theta = 0^\circ$ and reaches maximum value at $\theta = 90^\circ$. This phenomenon can be explained that the axial, flexural, torsional and shearing rigidities decrease significantly with increasing fiber angle, and thus, the relative geometrical nonlinear effect becomes larger for the higher fiber angles.

To investigate the geometrical nonlinear effect further, the same configuration with the previous example except in this case, the stacking sequence at two specific fiber angles $\theta = 45^\circ$ and 90° is considered to study the effects of load parameter on the displacements in the high nonlinear region. Load versus the vertical and torsional displacement of two fiber angles are shown in Figs.8 and 9. It is evident that linear analysis is not able to predict accurately the structural response where the applied load is larger than $\overline{q} = 1.0$ for fiber angle $\theta = 90^\circ$ and 1.5 for fiber angle $\theta = 45^\circ$, respectively. It is noteworthy that the results by nonlinear analysis are always larger than those of linear one. This is due to the fact that the geometrical nonlinear effect causes the axial-flexural-torsional-shearing coupling which results in a decrease in the flexural and torsional stiffness of the beam. The significant influence of the nonlinear analysis effect is easily verified with increasing load intensity. At the highest load of fiber angle $\theta = 45^\circ$, the nonlinear vertical and torsional displacements are about 165% and 125% of the linear values. Figs.10 and 11 clearly highlight the influence of geometrical nonlinear effect on the axial and lateral displacement of beam. These responses are never seen in linear analysis, as expected. It implies that a thin-walled composite beam under an eccentric transverse load not only causes the transverse displacement and angle of twist as would be observed in linear case, but also causes two additional responses due solely to geometric nonlinearity which does not occur in linear case.

VIII. CONCLUDING REMARKS

A geometrical nonlinear analysis of thin-walled composite beams with arbitrary lay-ups under various types of loads is presented. This model is based on the first-order shear deformable beam theory, and accounts for all the structural coupling coming from both material anisotropy and geometric nonlinearity. The general nonlinear governing equations are derived and solved by means of an incremental Newton-Raphson method. A displacement-based one-dimensional finite element model with seven-degree-of-freedom per node that accounts for the geometric nonlinearity in the von Kármán sense is developed. Numerical results are obtained to investigate the effects of fiber orientation, geometric nonlinearity and shear deformation on the axial-flexural-torsional response. The shear effects become significant for lower span-to-height ratio. The present model is found to be appropriate and efficient in analyzing geometrically nonlinear behavior of thin-walled composite beams under external loads.

Acknowledgments

The support of the research reported here by Basic Science Research Program through the National Research Foundation of Korea (NRF) funded by the Ministry of Education, Science and Technology (2009-0087819) is gratefully acknowledged.

References

[1] Vlasov, V. Z. (1961) *Thin Walled Elastic Beams*. Israel Program for Scientific Transactions, Jerusalem.

[2] Gjelsvik, A. (1981) *The theory of thin walled bars*. Wiley, New York.

[3] Bauld, N. R. and Tzeng, L. S. (1984) A Vlasov theory for fiber-reinforced beams with thin-walled open cross sections. *Int J Solids Struct*, **20**, 277 – 297.

[4] Gupta, R. K. and Rao, K. P. (1985) Instability of laminated composite thin-walled open-section beams. *Compos Struct*, **4**, 299 – 313.

[5] Gupta, R. K., Venkatesh, A., and Rao, K. P. (1985) Finite element analysis of laminated anisotropic thin-walled open-section beams. *Compos Struct*, **3**, 19 – 31.

[6] Stemple, A. D. and Lee, S. W. (1989) A finite element model for composite beams undergoing large deflection with arbitrary cross-sectional warping. *Int J Numer Meth Eng*, **28**, 2143–2160.

[7] Stemple, A. D. and Lee, S. W. (1989) Large deflection static and dynamic finite element analyses of composite beams with arbitrary cross-sectional warping. *AIAA, ASME, ASCE, AHS, and ASC, Structures, Structural Dynamics and Materials*

Conference, 30th, Mobile, AL, Technical Papers. Part 4, pp. 1788-1798.

[8] Omidvar, B. and Ghorbanpoor, A. (1996) Nonlinear FE Solution for Thin-Walled Open-Section Composite Beams. *J Struct Eng*, **122**, 1369–1378.

[9] Fraternali, F. and Feo, L. (2000) On a moderate rotation theory of thin-walled composite beams. *Compos Part B-Eng*, **31**, 141 – 158.

[10] Rajasekaran, S. and Nalinaa, K. (2005) Stability and vibration analysis of non-prismatic thin-walled composite spatial members of generic section. *Int J Struct Stab Dy*, **5**, 489–520.

[11] Bhaskar, K. and Librescu, L. (1995) A geometrically non-linear theory for laminated anisotropic thin-walled beams. *Int J Eng Sci*, **33**, 1331 – 1344.

[12] Librescu, L. and Song, O. (2006) *Thin-Walled Composite Beams: Theory and Application (Solid Mechanics and Its Applications)*. Kluwer Academic Pub.

[13] Machado, S. P. and Cortinez, V. H. (2005) Non-linear model for stability of thin-walled composite beams with shear deformation. *Thin-Walled Struct*, **43**, 1615 – 1645.

[14] Cortinez, V. H. and Piovan, M. T. (2006) Stability of composite thin-walled beams with shear deformability. *Comput Struct*, **84**, 978 – 990.

[15] Sapountzakis, E. J. and Panagos, D. G. (2008) Shear deformation effect in non-linear analysis of composite beams of variable cross section. *Int J Nonlinear Mech*, **43**, 660–682.

[16] Cardoso, J. B., Benedito, N. M., and Valido, A. J. (2009) Finite element analysis of thin-walled composite laminated beams with geometrically nonlinear behavior including warping deformation. *Thin-Walled Struct*, **47**, 1363–1372.

[17] Lee, J. (2005) Flexural analysis of thin-walled composite beams using shear-deformable beam theory. *Compos Struct*, **70**, 212 – 222.

[18] Vo, T. P. (2009) Linear and nonlinear finite element analysis of thin-walled composite structures. PhD thesis, Sejong University, Seoul, South Korea.

[19] Jones, R. M. (1999) *Mechanics of Composite Materials*. Taylor & Francis.

[20] Reddy, J. N. (2004) *An Introduction to Nonlinear Finite Element Analysis*. Oxford University Press.

[21] Kim, N. I., Shin, D. K., and Kim, M. Y. (2008) Flexural-torsional buckling loads for spatially coupled stability analysis of thin-walled composite columns. *Adv Eng Softw*, **39**, 949 – 961.

[22] Vo, T. P. and Lee, J. (2009) Flexural-torsional coupled vibration and buckling of thin-walled open section composite beams using shear-deformable beam theory. *Int J Mech Sci*, **51**, 631–641.

[23] ABAQUS (2004) *Standard user's manual. Ver 6.5-1*. Hibbitt, Karlsson & Sorensen Inc.

[24] Vo, T. P. and Lee, J. (2010) Geometrically nonlinear analysis of thin-walled open-section composite beams. *Comput Struct*, In Press.

CAPTIONS OF TABLES

Table I: Critical bucking loads (N) of a cantilever and simply supported mono-symmetric composite I-beam with symmetric angle-ply laminates in the flanges and web.

Table II: The tip axial and vertical displacements of a cantilever doubly symmetric composite I-beam with symmetric angle-ply laminates in the flanges and web under a vertical load P= 2000N at free end.

CAPTIONS OF FIGURES

Figure 1: Definition of coordinates and generalized displacements in thin-walled open-sections.

Figure 2: Load versus the lateral displacement at mid-span of a simply supported mono-symmetric composite I-beam under different values of initial loading imperfections with the fiber angles 30° and 60° in the flanges and web.

Figure 3: Load versus the lateral displacement at free end of a cantilever mono-symmetric composite I-beam under different values of initial loading imperfections with the fiber angles 30° and 60° in the flanges and web.

Figure 4: A pinned-hinged composite I-beam under an eccentric uniform load.

Figure 5: Variation of the highest load with respect to fiber angle change in the bottom flange of a pinned-hinged composite I-beam under an eccentric uniform load.

Figure 6: Variation of axial and horizontal displacement at mid-span with respect to fiber angle change in the bottom flange of a pinned-hinged composite I-beam under an eccentric uniform load.

Figure 7: Variation of the vertical displacement at mid-span with respect to fiber angle change in the bottom flange of a pinned-hinged composite I-beam under an eccentric uniform load.

Figure 8: Load versus the vertical displacement at mid-span of a pinned-hinged composite I-beam under an eccentric uniform load with the fiber angles 45° and 90° in the bottom flange.

Figure 9: Load versus the angle of twist at mid-span of a pinned-hinged composite I-beam under an eccentric uniform load with the fiber angles 45° and 90° in the bottom flange.

Figure 10: Load versus the axial displacement at mid-span of a pinned-hinged composite I-beam under an eccentric uniform load with the fiber angles 45° and 90° in the bottom flange.

Figure 11: Load versus the horizontal displacement at mid-span of a pinned-hinged composite I-beam under an eccentric uniform load with the fiber angles 45° and 90° in the bottom flange.

TABLE I Critical bucking loads (N) of a cantilever and simply supported mono-symmetric composite I-beam with symmetric angle-ply laminates in the flanges and web.

Lay-ups	Cantilever beam				Simply supported beam	
	Kim et al. [21]		Vo and Lee [22]	Present	Vo and Lee [22]	Present
	ABAQUS	Theory				
$[0]_{16}$	2969.7	2998.2	2993.2	2992.0	8918.1	8916.0
$[15/-15]_{4s}$	2790.9	2811.8	2803.6	2802.0	8587.7	8586.0
$[30/-30]_{4s}$	2190.6	2199.7	2184.7	2184.0	7187.1	7186.0
$[45/-45]_{4s}$	1558.9	1561.9	1546.0	1544.0	5352.0	5350.0
$[60/-60]_{4s}$	1239.4	1241.3	1277.8	1228.0	4291.9	4290.0
$[75/-75]_{4s}$	1132.2	1134.5	1126.7	1126.0	3898.4	3898.0
$[90/-90]_{4s}$			1106.8	1106.0	3893.4	3892.0

TABLE II The tip axial and vertical displacements of a cantilever doubly symmetric composite I-beam with symmetric angle-ply laminates in the flanges and web under a vertical load P= 2000N at free end.

Lay-ups	Formulation	W (cm)	V (cm)
$[0]_{16}$	ABAQUS	-0.152	11.414
	Present	-0.133	10.569
$[15/-15]_{4s}$	ABAQUS	-0.177	12.300
	Present	-0.161	11.649
$[30/-30]_{4s}$	ABAQUS	-0.300	15.921
	Present	-0.288	15.561
$[45/-45]_{4s}$	ABAQUS	-0.605	22.528
	Present	-0.597	22.364
$[60/-60]_{4s}$	ABAQUS	-0.965	28.422
	Present	-0.953	28.250
$[75/-75]_{4s}$	ABAQUS	-1.153	31.088
	Present	-1.126	30.724
$[90/-90]_{4s}$	ABAQUS	-1.202	31.758
	Present	-1.163	31.235

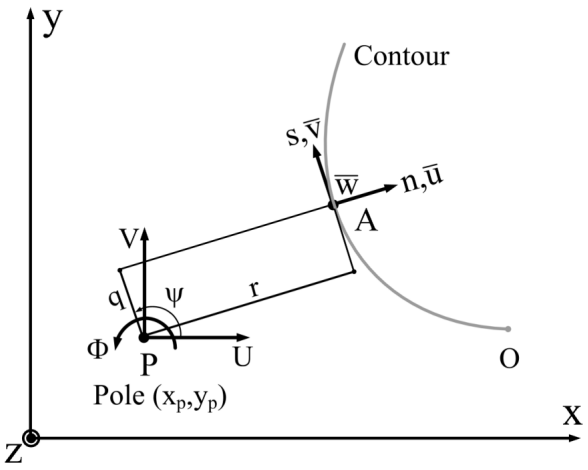

FIG. 1 Definition of coordinates and generalized displacements in thin-walled open-sections.

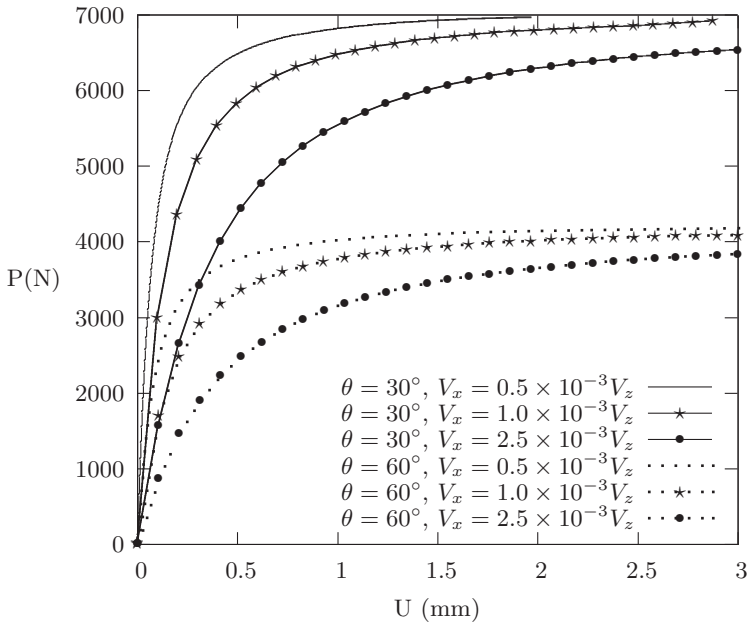

FIG. 2 Load versus the lateral displacement at mid-span of a simply supported mono-symmetric composite I-beam under different values of initial loading imperfections with the fiber angles 30° and 60° in the flanges and web.

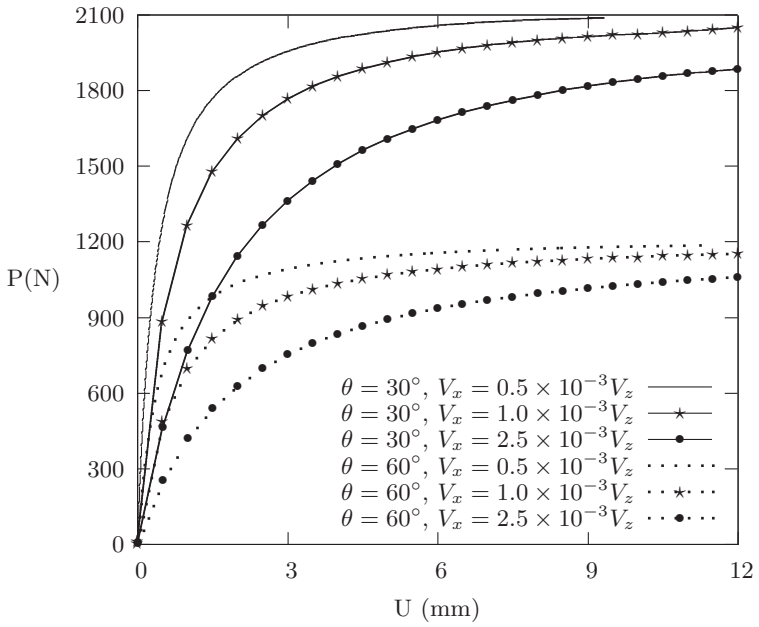

FIG. 3 Load versus the lateral displacement at free end of a cantilever mono-symmetric composite I-beam under different values of initial loading imperfections with the fiber angles 30° and 60° in the flanges and web.

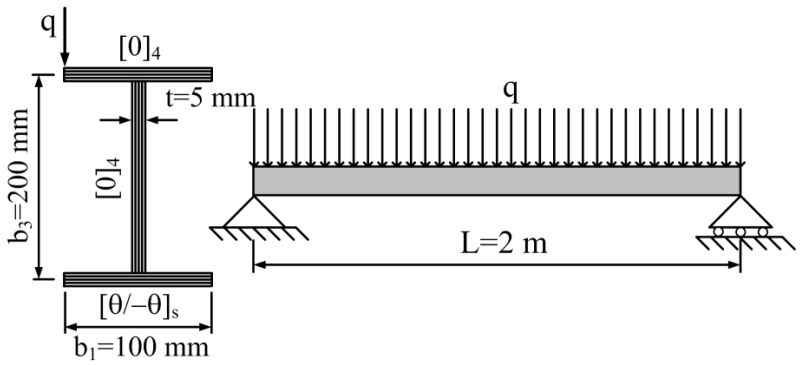

FIG. 4 A pinned-hinged composite I-beam under an eccentric uniform load.

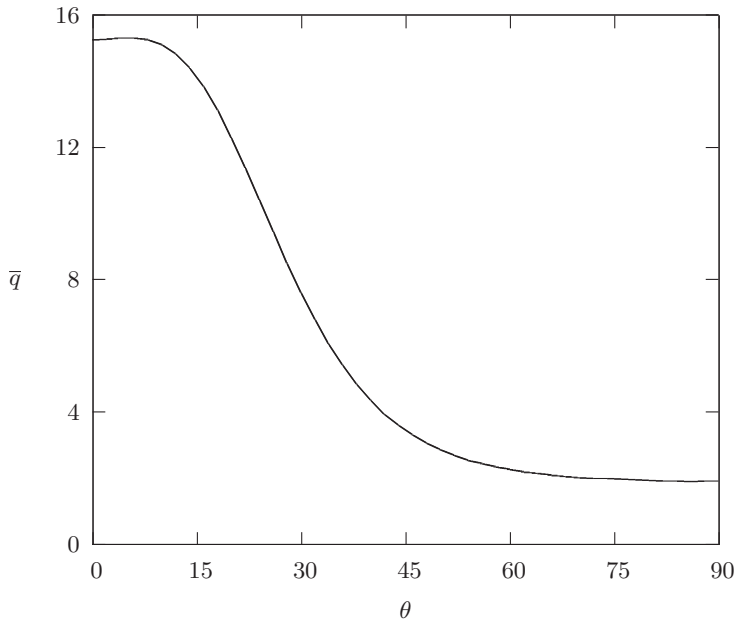

FIG. 5 Variation of the highest load with respect to fiber angle change in the bottom flange of a pinned-hinged composite I-beam under an eccentric uniform load.

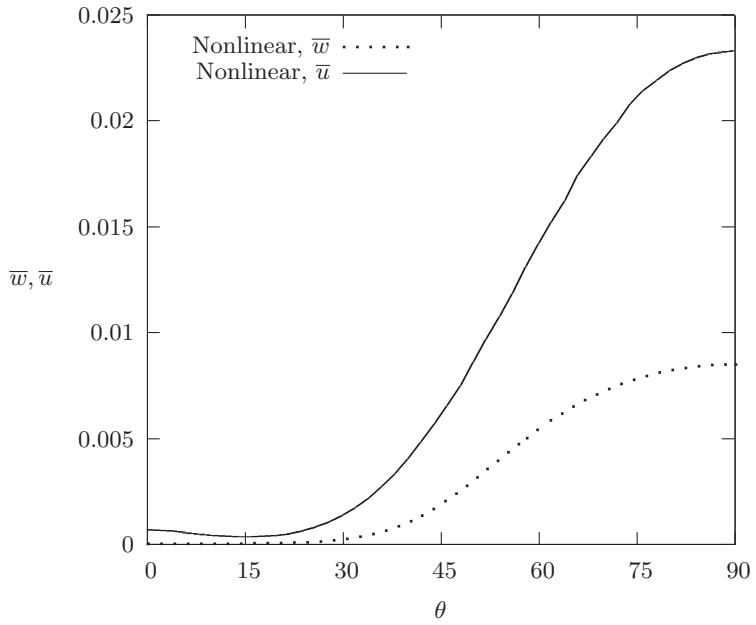

FIG. 6 Variation of axial and horizontal displacement at mid-span with respect to fiber angle change in the bottom flange of a pinned-hinged composite I-beam under an eccentric uniform load.

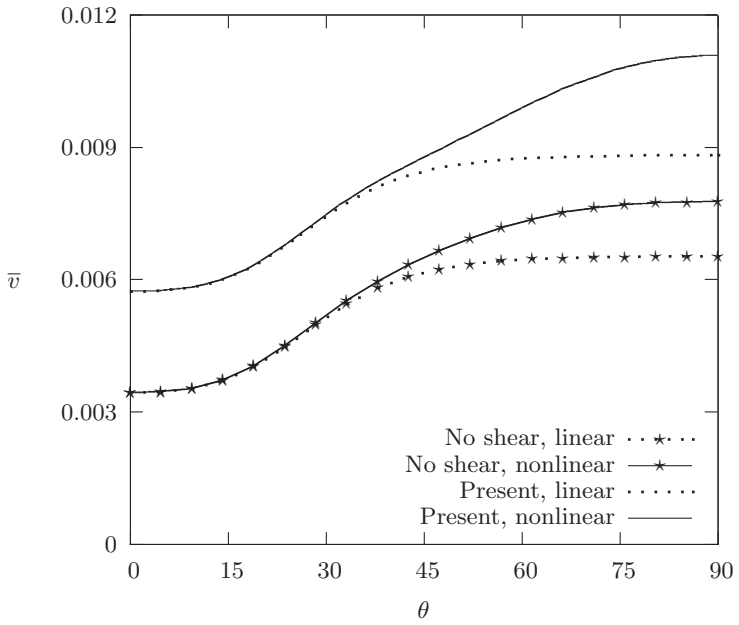

FIG. 7 Variation of the vertical displacement at mid-span with respect to fiber angle change in the bottom flange of a pinned-hinged composite I-beam under an eccentric uniform load.

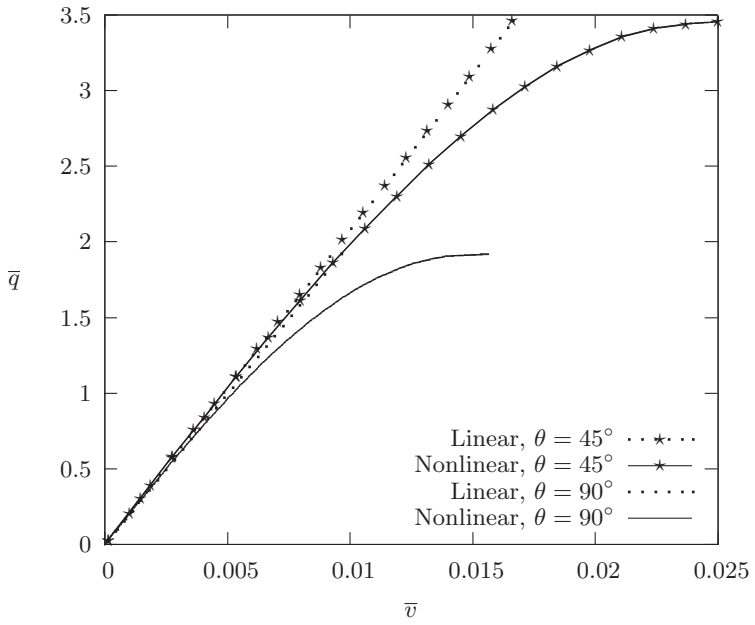

FIG. 8 Load versus the vertical displacement at mid-span of a pinned-hinged composite I-beam under an eccentric uniform load with the fiber angles 45° and 90° in the bottom flange.

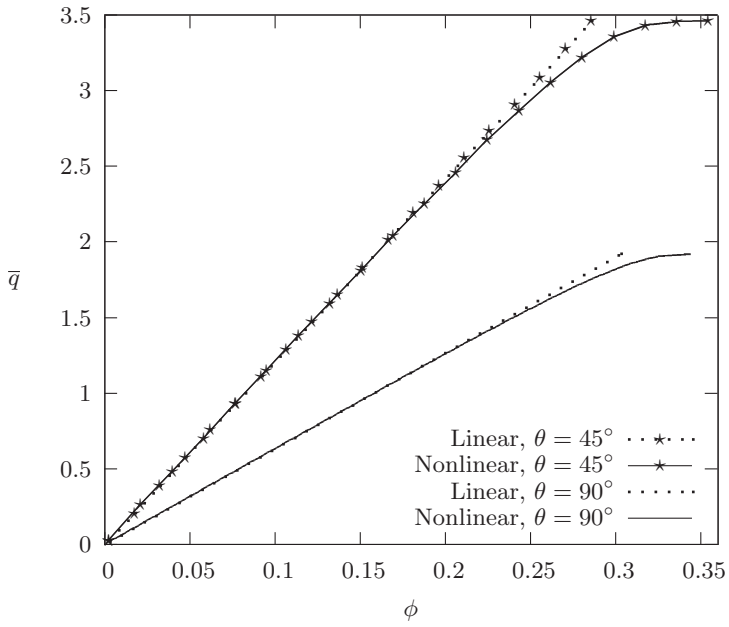

FIG. 9 Load versus the angle of twist at mid-span of a pinned-hinged composite I-beam under an eccentric uniform load with the fiber angles 45° and 90° in the bottom flange.

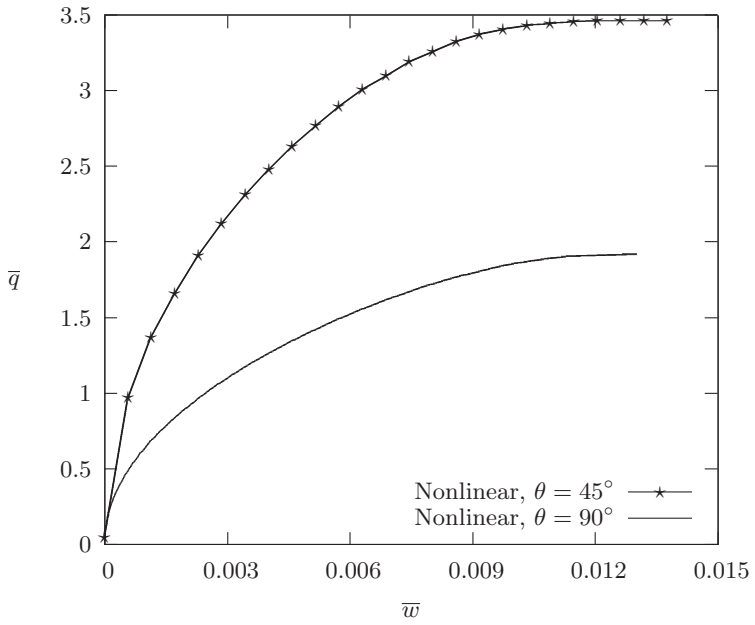

FIG. 10 Load versus the axial displacement at mid-span of a pinned-hinged composite I-beam under an eccentric uniform load with the fiber angles 45° and 90° in the bottom flange.

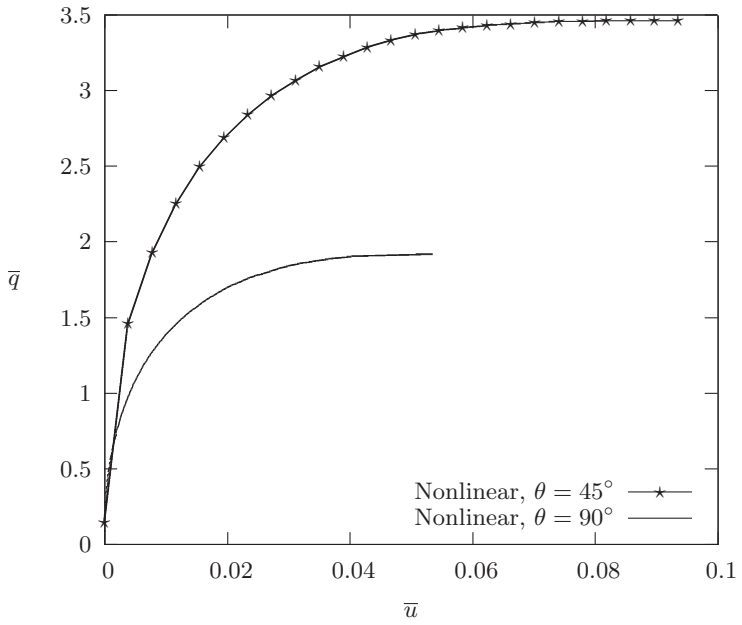

FIG. 11 Load versus the horizontal displacement at mid-span of a pinned-hinged composite I-beam under an eccentric uniform load with the fiber angles 45° and 90° in the bottom flange.